

## 8 *Passive Surface Wave Analysis*

---

Oh, that Einstein, always missing lectures - I really would not have believed him capable of it!

Hermann Minkowski

### 8.1 Introduction

Analysis of passive seismic surface waves, e.g. microtremors and traffic energy, offers several advantages over active surface wave tests, but requires more difficult signal processing procedures. In some cases, passive surface waves propagate with longer wavelengths, due to energy content in frequencies lower than those produced by active sources. Since the ambient wavefield is measured with an array of sensors simultaneously, the assumptions concerning noise and signal are more straight forward. The major advantages of the passive surface wave methods is that no source must be deployed and that measurements are typically conducted in the far-field.

### 8.2 Rayleigh Surface Waves from Passive Sources

The general wave propagation model given in Chapter 7 equals

$$u(\mathbf{k}, \mathbf{x}, \omega, t) = A_0(\mathbf{k}, \omega) e^{-\alpha(\mathbf{k}, \omega) \mathbf{x}} e^{j\omega t} R(\mathbf{k}, \mathbf{x}) \quad (8.1)$$

For the passive plane wave source, the model simplifies to

$$u(\mathbf{k}, \mathbf{x}, \omega, t) = A_0(\mathbf{k}, \omega) e^{-\alpha(\mathbf{k}, \omega) \mathbf{x}} e^{j\omega t} e^{-j(\mathbf{k} \cdot \mathbf{x})} \quad (8.2)$$

where the previously defined function  $R(\mathbf{k}, \mathbf{x})$  equals a complex exponential. Recall in the cylindrical wave propagation case,  $R(\mathbf{k}, \mathbf{x})$  controlled geometric spreading and phase change. In the plane wave case, the complex exponential contains only phase change information, since plane wave propagation does not spread geometrically.

At a fixed time and temporal frequency, the measurement between two reference points in a plane wavefield equals

$$\frac{u(\mathbf{k}, \mathbf{x}_2)}{u(\mathbf{k}, \mathbf{x}_1)} = \frac{A_0 e^{-\alpha(\mathbf{k}) \mathbf{x}_2} e^{-j(\mathbf{k} \cdot \mathbf{x}_2)}}{A_0 e^{-\alpha(\mathbf{k}) \mathbf{x}_1} e^{-j(\mathbf{k} \cdot \mathbf{x}_1)}} = e^{-[\alpha(\mathbf{k})(\mathbf{x}_2 - \mathbf{x}_1)]} e^{-j(\mathbf{k} \cdot \mathbf{x}_2 - \mathbf{k} \cdot \mathbf{x}_1)} \quad (8.3)$$

Interpreting Equation 8.3 as a filter, the measurements at position  $\mathbf{x}_2$  equal the input at  $\mathbf{x}_1$  scaled by the material attenuation coefficient and phase shifted by the wavenumber.

### 8.3 Site Description - I85 Site (Atlanta, GA)

A cleared and graded site near the I85 highway in Atlanta, GA was chosen for the deployment of a 16 sensor circular array. The array geometry and spectral characteristics were discussed in Section 4.6. Figure 8.1 shows a schematic of the site layout and location of the array. The array radius was 9.1 m (30 ft). An example ambient wavefield frequency spectrum is shown in Figure 8.2.

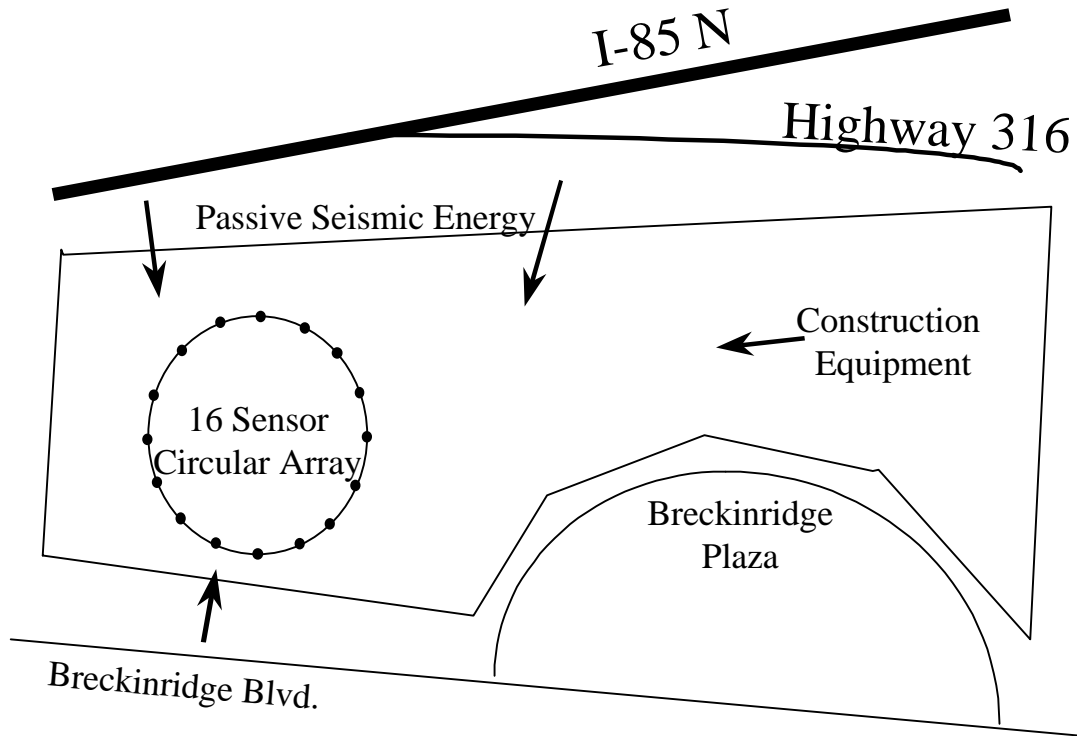


Figure 8.1 I85 Atlanta, GA Site Schematic

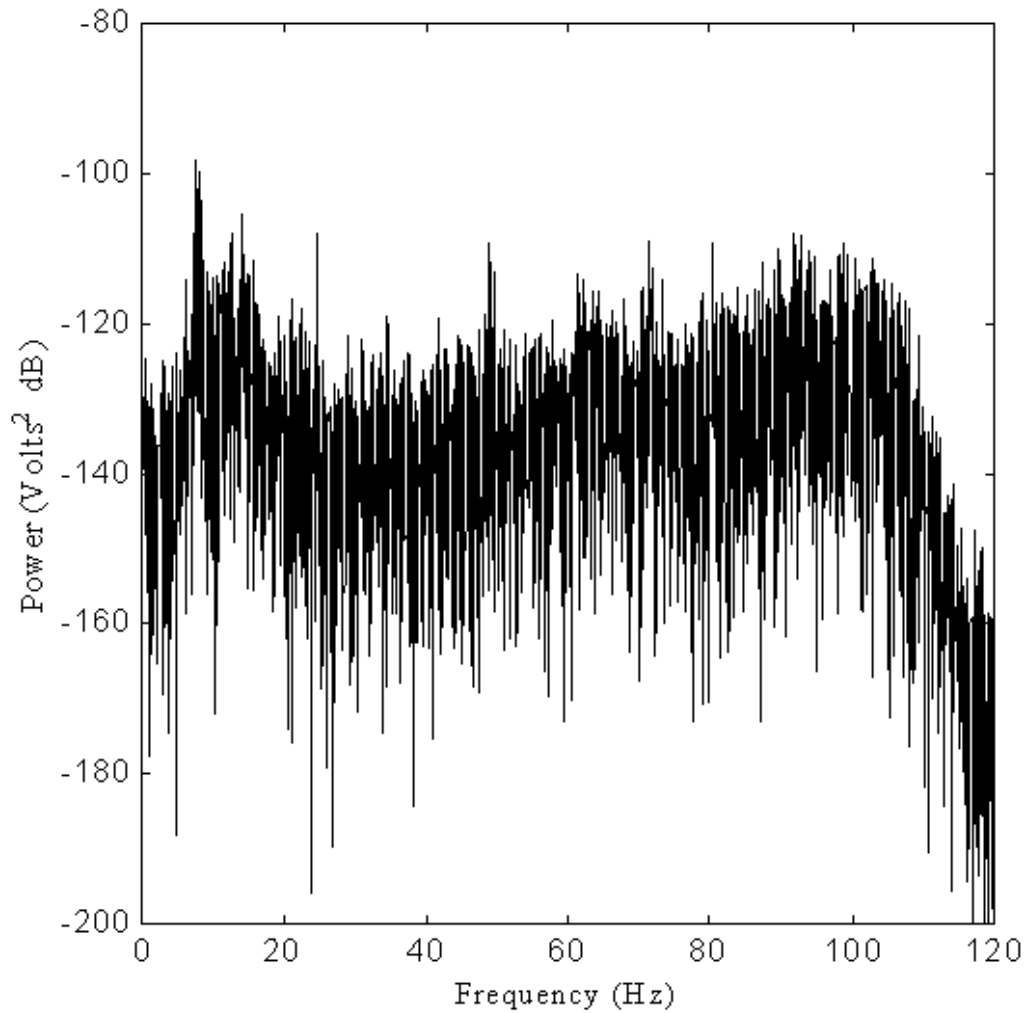


Figure 8.2 Temporal Power Spectrum for a Single Sensor at I85 Site

#### 8.4 Surface Wave Phase Velocity Estimation

Phase velocities from about 4 Hz to 55 Hz were estimated using the multidimensional power spectrum estimators discussed in Chapter 4. This section gives example power spectrum estimates, dispersion curve estimates, and discusses multiple signal arrivals and the direction of arrival as a function of frequency. The mesh plots of the power spectrums are useful to visualize the effects of the estimators on the spectrum background level.

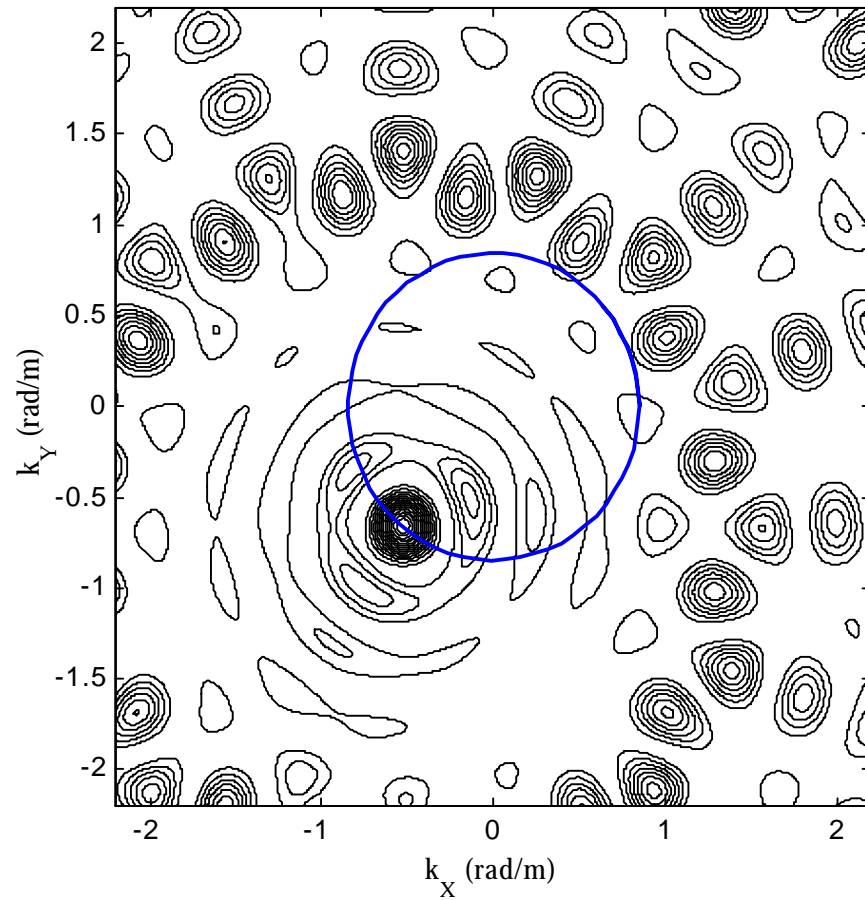


Figure 8.3 Passive Source FDBF  $f$ - $\mathbf{k}$  Power Spectrum Estimate at 24.5 Hz. Larger contours indicate greater energy estimates. The FDBF method estimated a phase velocity of 181.86 m/sec.

#### 8.4.1 FDBF

The FDBF frequency-wavenumber power spectrum estimate for frequency = 24.5 Hz is shown in Figures 8.3 and 8.4. A single dominant peak exists at wavenumber magnitude 0.846 rad/m. The sidelobes are clearly seen in the contour plot, and the mesh plot in Figure 8.4 yields perspective on the ripple of the wavenumber spectrum estimate. Figure 8.5 shows the FDBF estimate at 4.5 Hz. Although the spectrum exhibits a single peak, the relative radius of the peak compared to the wavenumber magnitude is large due to the limited resolution of the array. Figure 8.6 shows the FDBF estimated dispersion curve. The limited resolution of the array means the lower frequency phase velocity estimates probably are a mix of more than a single mode. At about 30 Hz, the dispersion curve begins to resolve additional modes. Figure 8.7 shows a close-up of the dispersion curve for lower frequencies.

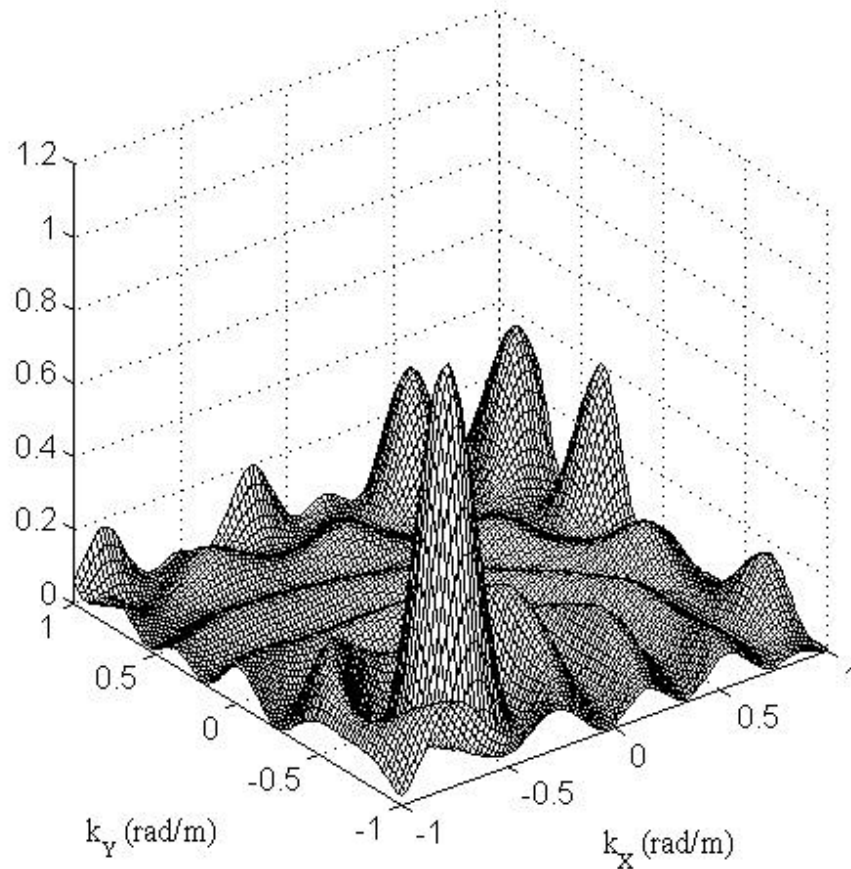


Figure 8.4 Mesh Plot of FDBF  $f$ - $\mathbf{k}$  Estimate at 24.5 Hz

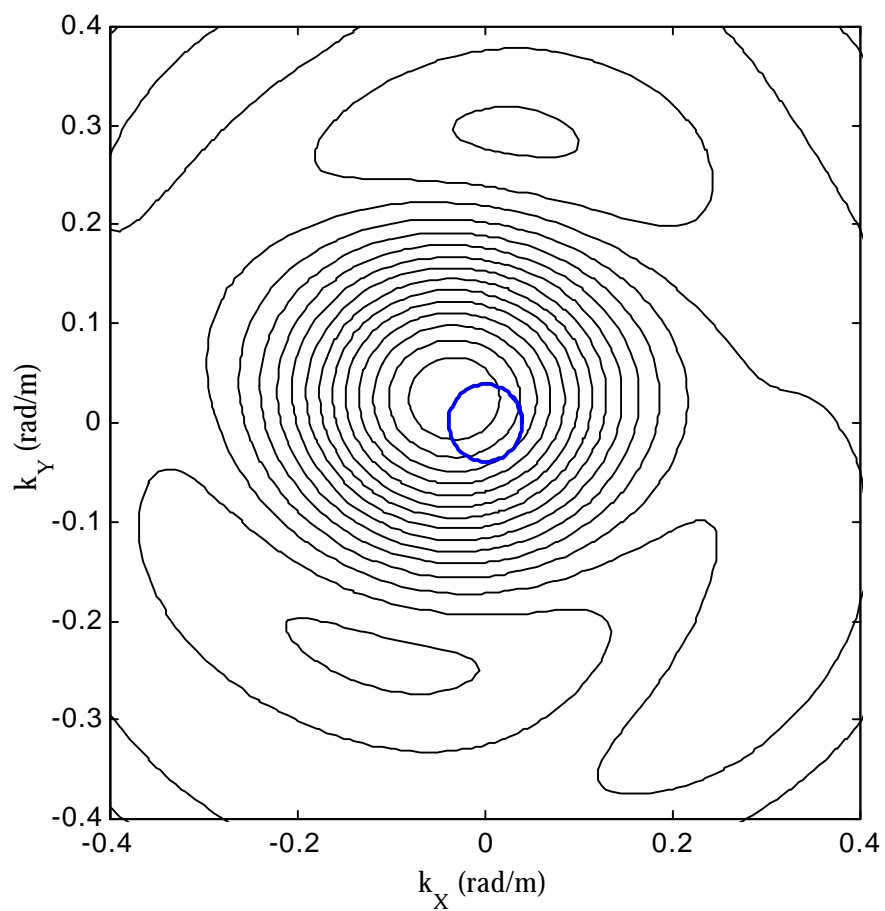


Figure 8.5 FDBF f- $\mathbf{k}$  Power Spectrum Estimate at 4.5 Hz. The peak in the power spectrum corresponds to a phase velocity of 724.03 m/sec.

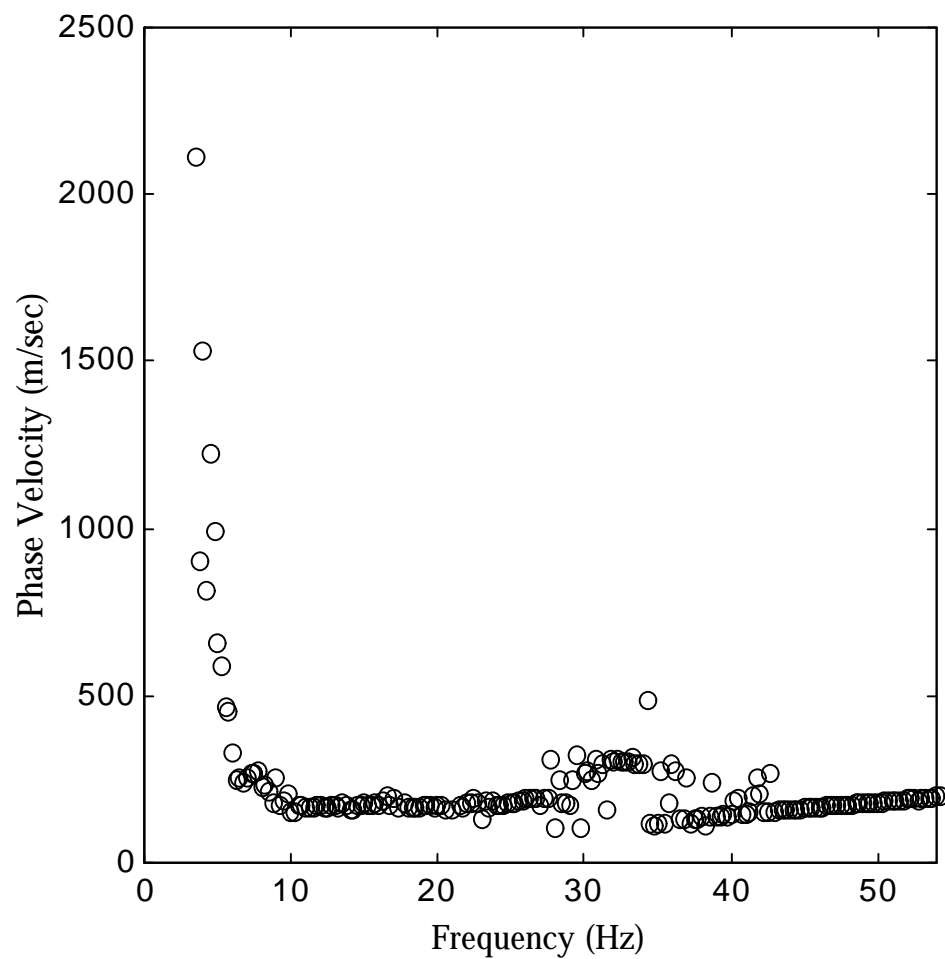


Figure 8.6 FDBF Dispersion Curve Estimate

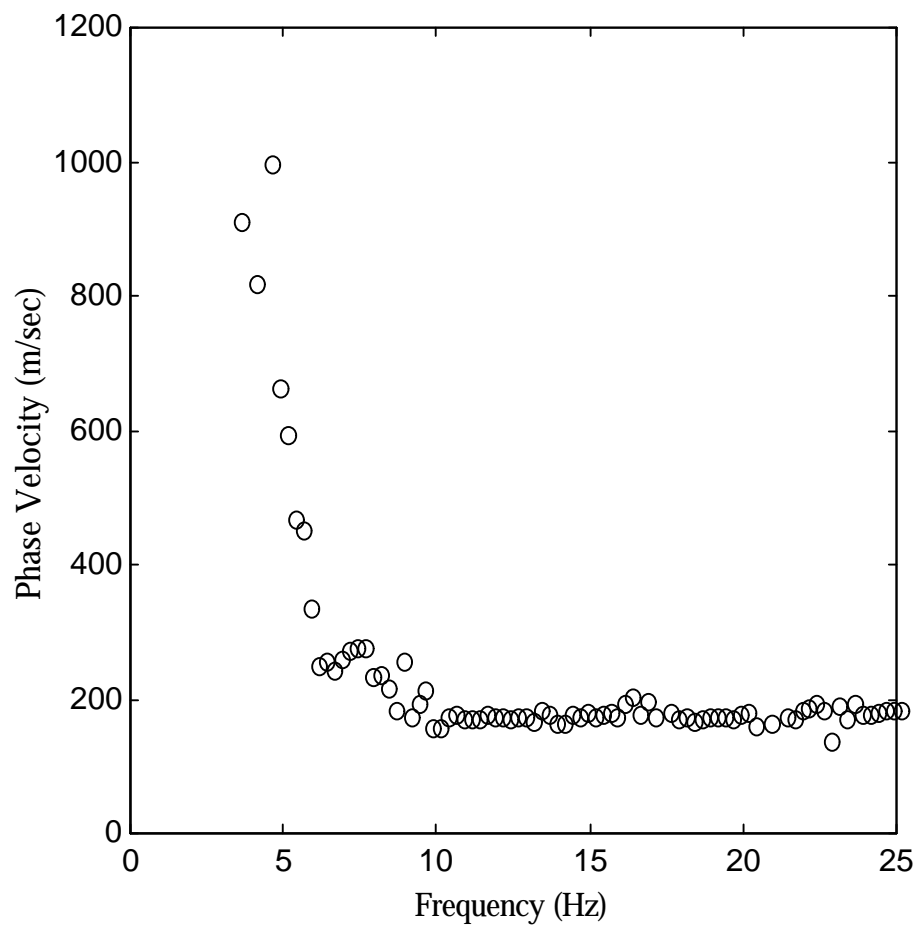


Figure 8.7 Close-Up of FDBF Estimated Dispersion Curve



#### 8.4.2 MVDL

The MVDL frequency-wavenumber power spectrum estimate for frequency = 24.5 Hz is shown in Figures 8.8 and 8.9. The MVDL method estimates the same phase velocity as the FDBF, but the signal related peak is much sharper and the background power estimate is much smoother. Figure 8.10 shows the MVDL estimated dispersion curve, and Figure 8.11 shows a close-up of frequencies up to 25 Hz. The MVDL and FDBF dispersion curves are very similar, except the MVDL yields more scattered estimates at low and high frequencies. The scatter may be explained by the underlying distribution of eigenvalues, since the MVDL will be more sensitive to convergence of the eigenvalues in the estimated inverse spatio-spectral correlation matrix. The increased scatter of the MVDL estimate is not surprising, since Seligson (1970) showed the FDBF will exhibit greater resolution in some cases.

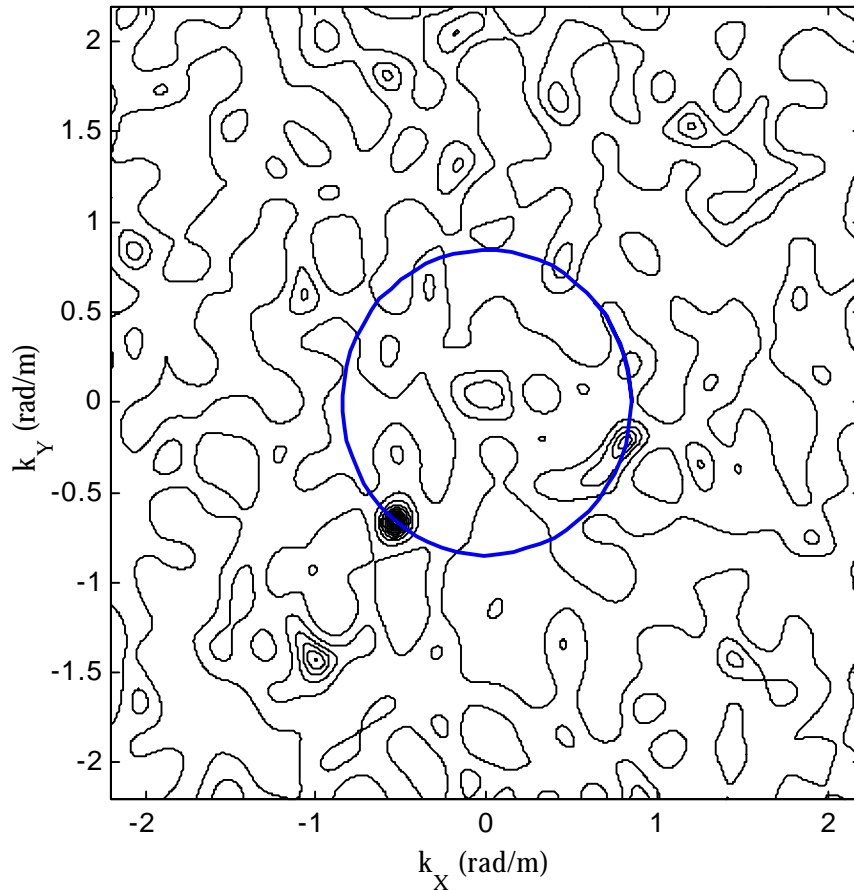


Figure 8.8 Passive Source MVDL f-**k** Power Spectrum Estimate at 24.5 Hz. The MVDL method estimated a phase velocity of 181.86 m/sec.

### 8.4.3 MUSIC

The MUSIC frequency-wavenumber power spectrum estimate for frequency = 24.5 Hz and noise subspace dimension = 15 is shown in Figures 8.12 and 8.13. MUSIC estimates the same phase velocity as the FDBF and MVDL methods, but the background level is much smoother, which is especially evident in the mesh plot, and the signal related peak is much narrower than the FDBF estimate. The estimate for a noise subspace dimension = 8 is shown in Figure 8.14. With a smaller noise subspace dimension, the power spectrum estimate exhibits greater ripple and spurious peaks. Figure 8.15 shows the MUSIC estimated dispersion curve. The dispersion curve exhibits less scatter than the MVDL method and is very similar to the FDBF method. Figure 8.16 shows a close-up of the MUSIC dispersion curve for lower frequencies.

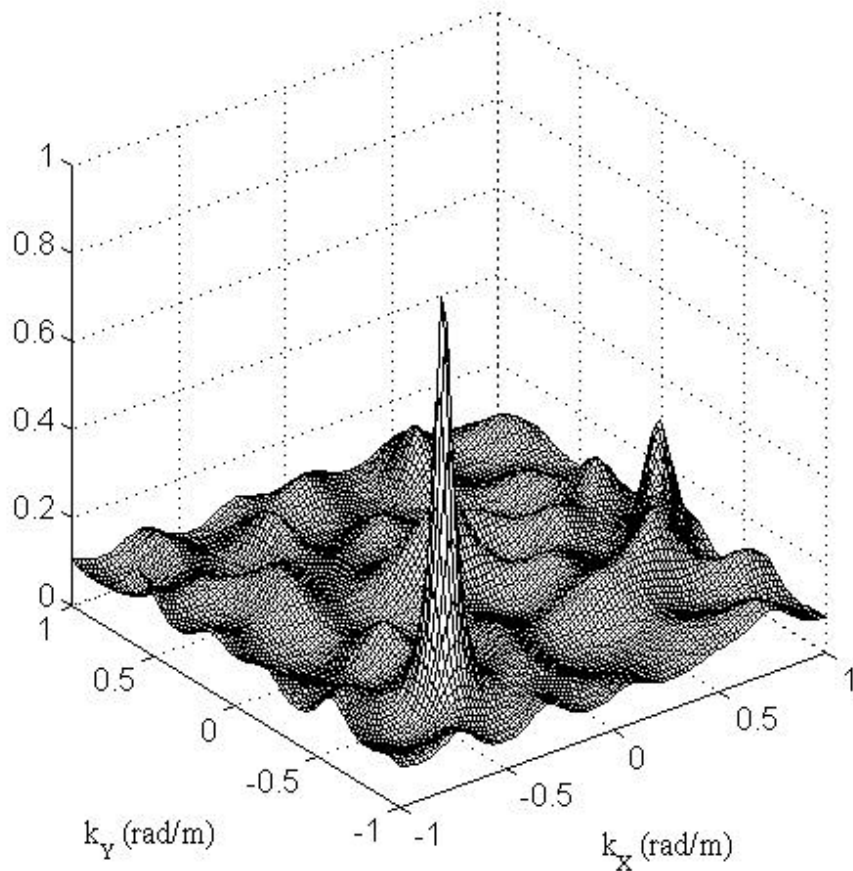


Figure 8.9 Mesh Plot of MVDL f-k Estimate at 24.5 Hz

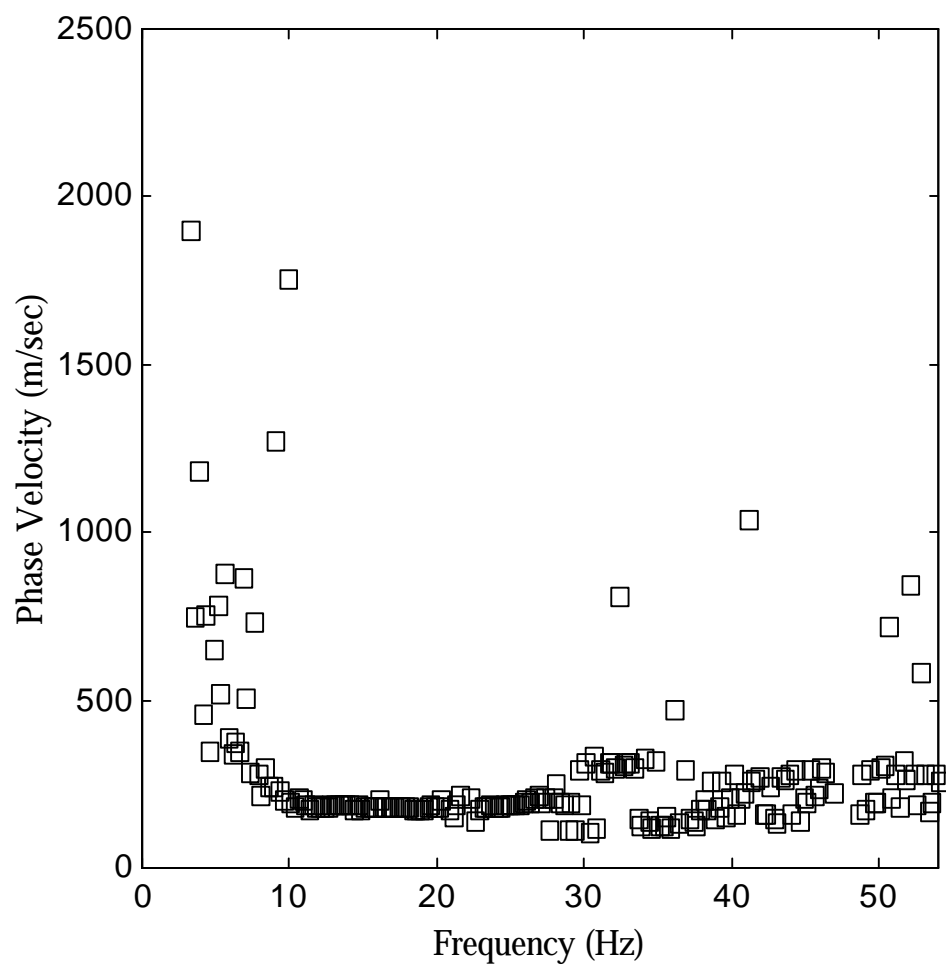


Figure 8.10 MVDL Dispersion Curve Estimate